https://doi.org/10.1016/j.applthermaleng.2018.07.099

A visible-light responsive micro photocatalytic fuel cell with laterally arranged electrodes

Rong Chen[a,b]*, Ming Xia[a,b], Xun Zhu[a,b]*, Qiang Liao[a,b], Dingding Ye[a,b], Liang An[c]*, Youxu Yu[a,b], Long Jiao[a,b], Wei Zhang[a,b]

[a] Key Laboratory of Low-grade Energy Utilization Technologies and Systems (Chongqing University), Ministry of Education, Chongqing 400030, China

[b] Institute of Engineering Thermophysics, Chongqing University, Chongqing 400030, China

[c] Department of Mechanical Engineering, The Hong Kong Polytechnic University, Hung Hom, Kowloon, Hong Kong, China

*Corresponding author.

[a,b] Tel.: 0086-23-65103119; fax: 0086-23-65102474; e-mail: rchen@cqu.edu.cn (Rong Chen)

[a,b] Tel.: 0086-23-65102474; fax: 0086-23-65102474; e-mail: zhuxun@cqu.edu.cn (Xun Zhu)

[c] Tel.: 852-27667820; fax: 852-23654703; e-mail: liang.an@polyu.edu.hk (Liang An)

Abstract

A micro photocatalytic fuel cell with a visible-light responsive photoanode and the lateral arrangement of the electrodes at the same plane was developed to enable simultaneous organics degradation and electricity generation. The developed micro photocatalytic fuel cell was assessed by using methanol as a representative organic compound in the alkaline environment. It is shown that good visible-light response was achieved. The effects of the light intensity, methanol concentration, KOH concentration and liquid flow rate were also explored. Experimental results showed that when the light intensity was increased, the cell performance was improved due to more photo-excited electron-hole pairs. Upgrading the KOH concentration led to the increased performance due to more efficient capture of the holes and enhanced cathodic reaction and ion transport. The increase of the methanol concentration in the testing range led to

the improved performance as a result of the enhanced mass transport. The discharging performance was firstly increased and then decreased with increasing the liquid flow rate due to the competition of enhanced mass transfer and organics crossover.

Keywords: μPFC; Lateral arrangement; Visible-light responsive photoanode; Electricity generation

1 Introduction

Directly discharging wastewater into natural water body not only threatens the human health but also triggers unwanted ecological effects. Therefore, the environmental problem of water pollution has become one of the critical issues facing our planet [1-3]. For this reason, many methods have been developed, such as biodegradation [4, 5], adsorption [6, 7] and chemical oxidation [8]. However, traditional wastewater treatment methods are usually concerned with how to rapidly and efficiently degrade pollutants contained in the wastewater. Actually, these pollutants also contains plenty of chemical energy, which almost meets 1/3 demand of the global energy consumption per year [2]. Unfortunately, the above-mentioned technologies are unable to efficiently utilize plentiful chemical energy contained in the wastewater, resulting in the energy loss. In this case, it is urgent to seek for new and efficient methods to simultaneously remove pollutants and recover the chemical energy stored in the wastewater.

The photocatalytic fuel cell (PFC) is one of promising technologies to meet the above demand, in which the abundant semiconductors are employed to function as the photoanode. As a result, the capital cost of the PFC can be much lower than that of conventional fuel cell [9]. During the PFC working process, the electron/hole pairs are photo-excited in the semiconductors upon illumination [10, 11]. The photo-excited holes can oxidize most organic compounds [12-15], while the photo-exited electrons go through the external load to the cathode to complete the oxgen reduction reaction. Since most organic compounds can be degraded photocatalytically, not only the wastewater can be efficiently purified but also the electricity can be generated simultaneously by using solar energy. Therefore, the PFC technology has been regarded as a promising method to treat wastewater and generate clear energy simultaneously [16-18].

In the past, the development of highly active photocatalysts has received numerous attention towards the improvement in the PFC performance [19-21]. For instance, Antoniadou et al. used CdS to functionalize commercial nanocrystalline titania [22]. Shu et al. developed BiOI-based photoanode to generate electricity by using organic compounds [23]. Li et al. developed a photocatalytic fuel cell with a BiOCl/Ti photoanode and a Pt cathode for the dye degradation and electricity generation [24]. Li et al. developed a dual photoelectrode photocatalytic fuel cell with a TiO_2/Ti photoanode and a Cu_2O/Cu photocathode for hazardous organics treatment with simultaneous electricity generation [25]. In addition to the photocatalysts, the PFC

performance is also dependent of its cell structure design due to its effect on the photon and mass transport. Currently, most existing PFCs are referred to as bulk reactors [8-10]. Besides, Seger *et al.* [26, 27] developed a photoelectrochemical cell with a membrane electrode assembly design. Tang *et al.* [28] proposed a photocatalytic fuel cell with an aqueous-film rotating disk for the generation of hydrogen and electricity. However, conventional PFCs usually have large dimensions, which is not beneficial for the photon and mass transport. For this reason, microfluidics that has the advantages of enhanced mass transfer due to high surface-to-volume ratio [29, 30], has been incorporated into the photocatalytic technologies to improve the performance, such as wastewater treatment [17] and CO_2 photoreduction [31, 32]. Recently, Xia et al. [33] developed a micro membraneless and monolithic photocatalytic fuel cell with the bare TiO_2 photoanode and an air-breathing cathode, in which two electrodes were laterally arranged at the same plane. In this design, not only the ion exchange membrane was eliminated to reduce the cost and the issues associated with the membranes, but also the oxygen transport could be enhanced to improve the cell performance as compared to the oxygen-dissolved cathode. Moreover, this design allowed it to be easily fabricated and integrated with other microdevices [34, 35]. Besides, the lateral arrangement of the electrodes makes it possible to use the photocathode without two-side illumination. However, bare TiO_2 photoanode was employed in this work, which could only respond to the UV light. The UV light only accounts for 3-5% sunlight. Under such a circumstance, the solar energy could not be efficiently utilized. Therefore, the development of a visible-light responsive photoanode for this new type of PFC is

needed, by which the cell performance and solar energy utilization efficiency can be further improved. Aiming at this target, a visible-light responsive micro photocatalytic fuel cell (μPFC) with the lateral arrangement of two electrodes at the same plane was developed in this study. The developed μPFC was assessed by using methanol as a representative organics pollutant in an alkaline environment.

2 Experimental

2.1 Design and fabrication of μPFC with the laterally arranged electrodes

The design of the developed μPFC with the lateral arrangement was similar to the previous work, which was consisting of a cover, a photoanode, a cathode and a baseplate [33], as shown in Fig. 1a. The polydimethylsiloxane (PDMS) was used to fabricate the cover and the baseplate. The photoanode was made by coating TiO_2 nanoparticles (Aeroxide P25, Acros, Belgium) on the fluorine-doped SnO_2 (FTO) conducting glass (resistance 10 Ω per square, Xinyan Technology Co., China). Commercially-available carbon paper coated with Pt (DMFC Cathode, Alfa Aesar, Great Britain) was cut into the T-shape to function as the cathode. Each part was briefly introduced as follows. The cover with the built-in micro chambers functioned as the reaction chambers for both the electrodes. In this study, methanol was used as a representative organics pollutant to function as the fuel for the PFC. Hence, methanol and electrolyte mixture was supplied into the photoanode chamber from the triangular-shape inlet and discharged out from the triangular-shape outlet, while the electrolyte was supplied into the cathode chamber. Depth of both the chambers was 0.9 mm. There

existed a line-shape convex in the middle at the cover plate. The convex had the depth of 0.4 mm. Due to the existences of the line-shape convex and triangular-shape inlets and outlets, the uniform supply of methanol and electrolyte, and effective avoidance of the organics crossover from the photoanode to the cathode could be ensured. For the photoanode, the FTO conducting glass with the dimension of 50 mm in length, 30 mm in width and 2.2 mm in thickness was employed. The conducting layer with 1 mm × 50 mm in the middle was removed to form an insulating region. The photocatalysts were coated on one side of the FTO conducting glass and a rectangle hole with 10 mm × 24 mm was drilled at the other side, which could be used to hold the cathode and breathe air. For the cathode, the straight region of the T-shaped Pt coated carbon paper was used, where the active area of the dimension of 24 mm × 4.5 mm was used for the cathodic reaction and the remaining region was used to collect the current. For the baseplate, it had the same dimension of 50 mm × 30 mm as the FTO conducting glass. Corresponding to the rectangle hole, a platform on the baseplate with the same size and location as the hole in the FTO conducting glass was designed, whose function was to hold the cathode and keep it at the same level with the photoanode. A rectangular hole with 20 mm in length and 3 mm in width was designed to provide the oxygen transport path from the ambient air. Fig.1b gives the picture of the fabricated μPFC.

2.2 Photoanode

The preparation of the visible-light responsive photoanode had four steps, including the laser drilling, etching, spraying and SILAR cycles. First, a 10 mm × 24 mm hole was

drilled in the FTO conducting glass by laser. Second, a 50 mm × 1 mm conduction layer in the middle of the FTO conducting glass was removed by the etching process, which could avoid the short circuit between the photoanode and cathode. Third, TiO_2 nanoparticles were sprayed onto the FTO conducting glass and then calcined for 2 hours at 550 °C to form a thin TiO_2 porous layer. Finally, the SILAR method was adopted to photo-sensitize the TiO_2 porous layer. To do this, two types of aqueous solution were needed. One was the solution with 0.075 mol/L $Cd(NO_3)_2$ (Aladdin, China) and 0.025 mol/L $Zn(NO_3)_2$ (Aladdin, China) and another one was the solution with 0.1 mol/L Na_2S (Aladdin, China). The TiO_2 coated FTO conducting glass was firstly put in the solution of $Cd(NO_3)_2$ and $Zn(NO_3)_2$ for 5 minutes and followed by washing with distilled water. Afterwards, the TiO_2 coated FTO conducting glass was put in the solution of Na_2S for 5 minutes and followed by washing with distilled water again, forming a SILAR cycle. Such cycle was repeated for 10 times. At last, the FTO conducting glass coated with CdS-ZnS/TiO_2 was baked at 100 °C for 10 minutes to form a visible-light responsive photoanode.

2.3 Performance evaluation instruments

During the experiment, the mixture of the methanol and KOH was supplied to the photoanode reaction chamber and the KOH electrolyte solution was pumped into the cathode reaction chamber using a two-channel syringe pump (Pump 33, Harvard, America), respectively. A 250 W Xe lamp (XD-300, Ningjing KWS Lighting, China) with AM 1.5G filter was employed as the solar irradiation source to simulate sunlight.

The light intensity was measured by a radiometer (FZ-A, Photoelectric Instrucment Factory of Beijing Normal University, China), which could be controlled by adjusting the distance between the μPFC and lamp. The polarization curve was measured by an electronic load system (CT-3008, Neware Technology Ltd., China). During the measurement of the polarization curve, each point was tested for 60 seconds. The photo-response behaviors were characterized by a data collecting instrument (34972A, Agilent, America). A UV-vis spectrophotometer (UV-2100, Shimadzu Corporation, Japan) was used characterize the UV-Vis spectra of the photoanode. The surface morphology of the photoanodes was characterized by the SEM (S-4800, Hitachi, Japan).

3 Results and discussion

3.1 Photoanode characterization

Fig. 2 shows the SEM images of the bare TiO_2 porous layer and the quantum-dots photosensitized TiO_2 porous layer. As shown in the Fig. 2a, for the bare TiO_2 porous layer, although the TiO_2 nanoparticles were easily agglomerated, forming the clusters, they were still distributed uniformly on the FTO conducting glass. After the photosensitization, CdS-ZnS spread in and between TiO_2 nanoparticles. The presence of CdS-ZnS was demonstrated by the formed large clusters, each of which consisted of ultra-small CdS and ZnS nanoparticles, as shown in Fig. 2b. This result indicated that the TiO_2 porous layer was uniformly coated by the CdS-ZnS. The UV-Vis spectra of the bare TiO_2 and CdS-ZnS/TiO_2 were also measured. As shown in Fig. 3, bare TiO_2 could only absorb the light with the wavelength of below 400 nm. However, the

absorbed wavelength of the CdS-ZnS/TiO_2 could reach about 550 nm, which implied that the use of CdS-ZnS for the photosensitization could effectively broaden the spectra of the photoanode, allowing it for the visible-light response.

3.2 Photoresponse behavior

In this study, the photoresponse behaviors of the developed μPFC were characterized by choosing the open circuit voltage (OCV) and short circuit current density (SCCD) as the representative cell voltage and current density, respectively. The operating conditions are the light intensity of 100 mW/cm^2, the methanol concentration of 1.0 M, the KOH concentration 0.5 M and the liquid flow rate of 200 μL/min at both the electrodes. The photovoltage-time curve and the photocurrent-time curve in response to the light on/off mode are presented in Fig. 4. It is seen from Fig. 4a that when the irradiation was initiated, the OCV was immediately jumped to about 1.3 V and then gradually to about 1.4 V. Once the light was switched off, the voltage was instantly down to about 0.6 V and then gradually to about 0.4 V. Such photoresponse behavior could be well reproduced in the tested three cycles. For the photocurrent response shown in Fig. 4b, when the light was turned on, the SCCD was immediately boosted to about 5.5 mA/cm^2 and then slowly increased to 5.6 mA/cm^2. Once the light was turned off, the SCCD was immediately decreased to about zero. The photocurrent response could also be well reproduced in the tested four cycles. These results implied that the developed μPFC with the lateral arrangement of the electrodes had good response to the solar irradiation.

3.3 Influence of light intensity

Obviously, the developed μPFC with the lateral arrangement of the electrodes can only work under the illumination because the photoanode reaction is actuated by the photo-excited electron/hole pairs, which highly depends on the intensity of incident light. As a consequence, the effect of the light intensity was firstly explored. Here, four light intensities of 40, 70, 100 and 130 mW/cm^2, were chosen. Methanol concentration was kept at 1.0 M, while the KOH concentration and liquid flow rates at both the electrodes were 0.5 M and 200 μL/min, respectively. The polarization curves and the corresponding power density curves are presented in Fig. 5. It was found that with the light intensity increasing from 40 mW/cm^2 to 130 mW/cm^2, the OCV and SCCD were increased from about 1.22 V to 1.34 V and from 2.1 mA/cm^2 to 7.3 mA/cm^2, respectively. This is because an increase in the light intensity could excite more electron-hole pairs, producing more hydroxyl radicals that had strong oxidability and thereby enhance the photoanode reaction to lift the cell performance [17]. It was also found that at high current density region, each polarization curve showed a sharp decrease. For example, at the light intensity was 100 mW/cm^2, when the current density was lower than about 5 mA/cm^2 with the corresponding cell voltage of about 0.74 V, the almost linear decline of the cell voltage was observed. Once the current density was larger than 5 mA/cm^2, the cell voltage began to sharply decrease. The possible reason might be that the cell voltage was too low at high current densities, which could not provide sufficient driving force for the electron transport from the photoanode to the cathode. In this case, the photo-excited electron-hole pairs were easily recombined so

that the amount of holes was reduced, leading to less hydroxyl radicals that are strong oxidant to be generated. Therefore, the lowered hydroxyl radicals concentration slowed down the photoeletrochemical reaction rate, which caused the cell voltage to be sharply decreased [17]. When the light intensity was increased to 130 mW/cm^2, a similar trend was found. The sharp drop of the cell voltage started at about 0.54 V. As compared to the cases of 40 mW/cm^2 and 70 mW/cm^2, it can be found that the cell voltage corresponding to the onset of the sharp drop was decreased. This might be due to the fact that the increased light intensity resulted in more electron-hole pairs to be generated. The increased amount of the generated electron-hole pairs could compensate the recombination resulting from the low cell voltage to some extent. Hence, the onset of the sharp voltage drop was decreased with increasing the light intensity. With the polarization curves, the variation in the power density with the photocurrent density was achieved. As presented in Fig. 5b, an increase in the light intensity led to the significant reduction in the peak power density from 1.34 mW/cm^2 to 4.27 mW/cm^2. These results implied that the light intensity is a critically important parameter to maximize the performance of the developed μPFC.

3.4 Influence of methanol concentration

The developed μPFC with the lateral arrangement of the electrodes can convert chemical energy stored in the organics into electricity by using the solar energy. In this case, the change of the supplied methanol concentration can affect the methanol concentration at the photoanode and thus the cell performance. Knowing how the

methanol concentration affects the cell performance is helpful to understand the capacity of the developed μPFC to degrade the organic compounds and generate the electricity. Therefore, the effect of the methanol concentration was studied. In this measurement, the operating conditions were the light intensity of 100 mW/cm^2, the KOH concentration of 0.5 M and the liquid flow rate of 200 μL/min at both the electrodes, respectively. The methanol concentration ranged from 0.05 M to 4.0 M. The results on the influence of the methanol concentration are shown in Fig. 6. It is seen from Fig. 6a that the OCV and SCCD became larger with increasing the methanol concentration. Specially, as the methanol concentration increased from the extremely low as 0.05 M to 1.0 M, the improvements in the SCCD and OCV were significant. This is because methanol can effectively scavenge the photo-excited holes to promote the photoelectochemical reactions [36]. When the methanol concentration was critically low, the mass transfer limitation was rather serious, resulting in an extremely low concentration at the photoanode. Under such a circumstance, the positive effect resulting from the supplied methanol was weak. As a consequence, the photoelectrochemical reaction occurring in the photoanode was greatly slowed down so that the SCCD and OCV were small. As the methanol concentration was upgraded to 1.0 M, this issue was well addressed. Therefore, the SCCD and OCV could be greatly improved. As the methanol concentration was further upgraded, the mass transport issue related to the methanol concentration was not so significant. However, the increased methanol concentration was still able to promote the photoanode reaction, but its contribution was lowered. On the other hand, the increase of the methanol

concentration might result in more severe methanol crossover to the cathode, which caused the increased mixed potential at the cathode and thus lowered the cathode potential. Therefore, these combined effects led to smaller increment of the cell performance at high methanol concentrations. Fig. 6b shows the corresponding power density curves. As shown, with the methanol concentration increasing from 0.05 M to 1.0 M, a significant increase in the peak power density from 2.03 mW/cm^2 to 3.71 mW/cm^2 was achieved. As the methanol concentration was further lifted to 4.0 M, the peak power density was gradually upgraded to 4.0 mW/cm^2. Based on the results on the influence of the methanol concentration, it can be found that increasing the methanol concentration facilitated the improvement in the cell performance, particularly at low methanol concentration operations.

3.5 Influence of the electrolyte concentration

The OH^- ions are good scavengers to capture the holes at the photoanode and facilitates the oxygen reduction reaction at the cathode. Hence, the electrolyte (KOH) concentration can greatly affect the photoelectrochemical/electrochemical reactions at both the electrodes. Moreover, the KOH concentration can influence the ion transfer between the electrodes and thereby the internal cell resistance. Therefore, the influence of the KOH concentration was also explored. In this measurement, the operating conditions were the methanol concentration of 1.0 M, and the light intensity of 100 mW/cm^2, and the liquid flow rate of 200 μL/min at both the electrodes. The KOH concentration ranged from 0.01 M to 1.0 M KOH. The results on the influence of the

electrolyte concentration are given in Fig. 7a. It was observed that as the KOH concentration increased, both the OCV and SCCD increased. Three reasons contributed to the increased performance. First, an increase in the KOH concentration resulted in the enhancement of the cathode reaction kinetics due to the decrease of the cathode overpotential [37, 38]. Second, the OH^- ions could function as the hole scavengers. An increase in the KOH concentration could capture more photo-excited holes so as to inhibit the recombination of the electron/hole pairs. In this case, the photoelectrochemical reactions at the photoanode were enhanced. Third, an increase in the KOH concentration enhanced the transfer of the OH^- ion, by which the internal cell resistance could be decreased. This could be evidenced by comparing the slopes of these polarization curves at the middle current density region. Because of the above reasons, the cell performance, including the OCV and SCCD, was lifted with an increase in the electrolyte concentration. Fig. 7b shows the power density against the current density at various KOH concentrations. It is seen that an increase in the KOH concentration from 0.01 M to 1.0 M led to the increase of the peak power density from 2.04 mW/cm^2 to 3.90 mW/cm^2. These facts imply that high electrolyte concentration is beneficial for improving the cell performance.

3.6 Influence of the liquid flow rate

Mass transfer also play an important role in the cell performance, which is also affected by the liquid flow rate. For this reason, the influence of the liquid flow rate was also investigated in this study. Here, the liquid flow rates at both the electrodes remained

the same and varied from 10 μL/min to 1200 μL/min. The methanol concentration, the KOH concentration at both the photoanode and cathode, and the light intensity were maintained at 1.0 M, 0.5 M and 100 mW/cm^2, respectively. Fig. 8 shows the variation of the cell performance with the liquid flow rate. As seen from Fig. 8a, with the liquid flow rate increasing from 10 μL/min to 200 μL/min, the cell performance including the OCV and SCCD was improved. However, as the liquid flow rate was further increased, the cell performance started to decline. At extremely low liquid flow rate of 10 μL/min, although the residence time was large, which facilitated the reactions, the methanol and KOH concentrations at the electrodes were low due to poor mass transfer. In this case, the photoelectrochemical/electrochemical reaction kinetics was restricted, leading to poor performance. When it was increased to 200 μL/min, the mass transport was enhanced so that this restriction was mitigated and the cell performance was enhanced. With the further increase of the liquid flow rate to 600 μL/min and 1200 μL/min, although the mass transport could be further enhanced, the residence time was greatly reduced, which lowered the reaction efficiency. Moreover, the methanol crossover became more severe, which lowered the cathode potential. Both these two effects negatively contributed to the cell performance. Therefore, the cell performance was firstly increased and then decreased as the liquid flow rate increased in the testing range. An optimal performance was achieved at the liquid flow rate of 200 μL/min in this work. A maximum peak power density of about 3.71 mW/cm^2 was yielded at this liquid flow rate, as seen in Fig. 8b. It should be pointed out that although the change of the liquid flow rate could affect the cell performance, its effect was not significant.

3.7 Long-term performance

Durability of the developed μPFC with the lateral arrangement of the electrodes is of importance for real applications. Because of this, the long-term performance was also studied, which was characterized by measuring the variation in the cell voltage with the running time at a given current density. In this study, the cell voltage vs the running time at 3.5 mA/cm^2 for more than 3 hours was tested. The other conditions were the methanol concentration of 1.0 M, the KOH concentration of 0.5 M, the light intensity of 100 mW/cm^2 and the liquid flow rate of 200 μL/min at both the photoanode and cathode. It was found from Fig. 9 that the voltage was relatively stable in the testing period. The voltage was only declined from 0.91 V to 0.84 V, which accounted for 8% drop. The possible reason might be the adsorption of the intermediates at the photocatalysts and the photocorrosion of CdS-ZnS during the long-term operation [39]. Generally speaking, the developed μPFC with the lateral arrangement of the electrodes developed in this study could show relatively stable performance. However, further improvement in the durability is still needed for future applications

4 Conclusions

A micro photocatalytic fuel cell with a visible-light responsive photoanode and the lateral arrangement of the electrodes at the same plane was developed in this study for simultaneously degrading organics and generating electricity. Photosensitizing the CdS-ZnS to TiO_2 allowed the photoanode to be responsive to the visible light. The evaluation of the developed μPFC was performed by using methanol as the

representative organic compound in the wastewater under various conditions. The UV-Vis spectra and photoresponse characterization proved that the developed μPFC could well respond to the visible light. Parametric study indicated that the increase of the light intensity and the electrolyte concentration could boost the performance as a result of more photo-excited electron-hole pairs, and more efficient capture of holes at the photoanode and enhanced cathodic reaction and ion transfer, respectively. An increase in the methanol concentration resulted in the improvement of the cell performance due to enhanced mass transport. Besides, although an increase in the liquid flow rate could facilitate the mass transport, the decreased residence time and increased methanol crossover brought negative contribution to the cell performance. The competition between the enhanced mass transport and decreased residence time and increased methanol crossover led to the best cell performance at a liquid flow rate of 200 μL/min in this work. However, the effect of the liquid flow rate was not so significant as compared to other operating parameters. By doing this parametric study, the optimized these parameters in the testing ranges could be achieved, which corresponded to the light intensity of 130 mW/cm^2, the methanol concentration of 4.0 M, the KOH concentration of 1.0 M and the liquid flow rate of 200 μL/min, respectively. The long-term discharging performance was also characterized and the results showed that the relatively stable performance of the developed μPFC with the lateral arrangement of the electrodes was obtained.

Acknowledgments

The authors gratefully acknowledge the financial supports of the National Natural Science Foundation of China (No. 51576021, No. 51620105011, No. 51506039 and No. 51776026) and the National High-Tech R&D Program of China (No. 2015AA043503).

References

[1] M. J. Kennish, *Environ. Conserv.* **2002**, *29*, 78-107.

[2] G. Tchobanoglous, F. L. Burton, H. D. Stensel, D. *Wastewater Engineering: Treatment and Resource Recovery, 5th ed.,* Metcalf & Eddy I AECOM, McGraw-Hill Book Company, New York, **2013**, 1-4

[3] A. O. Alade, A. T. Jameel, S. A. Muyubi, M. I. Abdul Karim, M. Zahangir Alam, *IIUM Eng. J*. **2011**, *12*, 161-169

[4] R. G. Qualls, B. L. Haines, *Soil Sci. Soc. Am. J.* **1992**, *56*, 578-586.

[5] A. Joss, Zabczynski S, Göbel A, B. Hoffmann, D. Loffler, C. S. McArdell, T. A. Ternes, A. Thomsen, H. Siegrist, *Water Res.* **2006**, *40*, 1686-1696.

[6] J. A. Davis, R. Gloor, *Environ. Sci. Technol*. **1981**, *15*, 1223-1229.

[7] M. R. Azhar, H. R. Abid, H. Q. Sun, V. Periasamy, M. O. Tade, S. B. Wang, *J. Colloid Interf. Sci.* **2016**, *478*, 344-352.

[8] M. Peña, M. Coca, G. González, R. Rioja, M. T. Garcia, *Chemosphere*, **2003**, *51*, 893-900.

[9] M. N. Chong, B. Jin, C. W. K. Chow, C. Saint, *Water Res*. **2010**, *44*, 2997-3027.

[10] H. Tong, S. X. Ouyang, Y. P. Bi, N. Umezawa, M. Oshikiri, J. H. Ye, *Adv. Mater.*

2012, *24*, 229-251.

[11] A. Fujishima, K. Honda, *Nature*. **1972**, *238*, 37-38.

[12] K. Pelentridou, E. Stathatos, H. Karasali, P. Lianos, *J. Hazard. Mater*. **2009**, *163*, 756-760.

[13] P. Lianos, *J. Hazard. Mater*. **2011**, *185*, 575-590.

[14] P. W. Huo, Y. S. Yan, S. T. Li, H. M. Li, W. H. Huang, *Desalination*. **2010**, *256*, 196-200.

[15] S. Sakthivel, B. Neppolian, M. V. Shankar, B. Arabindoo, M. Palanichamy, V. Murugesan, *Sol. Energ. Mat. Sol. C.* **2003**, *77*, 65-82.

[16] Y. B. Liu, J. H. Li, B. X. Zhou, X. J. Li, H. C. Chen, Q. P. Chen, Z. S. Wang, L. Li, J. L. Wang, W. M. Cai, *Water Res*. **2011**, 45, 3991-3998.

[17] L. Li, G. Y. Wang, R. Chen, X. Zhu, H. Wang, Q. Liao, Y. X. Yu, *Lab Chip*. **2014**, *14*, 3368-3375.

[18] M. Canterino, I. Di Somma, R. Marotta, R. Andreozzi, V. Caprio, *Water Res.* **2009**, *43*, 2710-2716.

[19] K. Li, H. B. Zhang, T. T. Tang, Y. L. Xu, D. W. Ying, Y. L. Wang, J. P. Jia, *Water Res*. **2014**, *62*, 1-10.

[20] M. Antoniadou, D. I. Kondarides, D. D. Dionysiou, P. Lianos, *J. Phys. Chem. C.* **2012**, *116*, 16901-16909.

[21] L. Li, R. Chen, X. Zhu, Q. Liao, H. Wang, L. An, M. X. Zhang, *J. Cataly*. **2016**, 344, 411-419.

[22] M. Antoniadou and P. Lianos, *J. Photoch. Photobio. A.* **2009**, 204, 69-74.

[23] D. Shu, J. Wu, Y. Gong, S. Li, L. Hu, Y. Yang, C. He, *Catal. Today.* **2014**, 224, 13-20.

[24] K. Li, Y. Xu, Y. He, C. Yang, Y. Wang, J. Jia, *Environ. Sci. Technol.* **2013**, 47, 3490-3497.

[25] J. Li, J. Li, Q. Chen, J. Bai, B. Zhou, *J. Harard. Mater.* **2013**, 262, 304-310.

[26] B. Seger, P. V. Kamat, *J. Phys. Chem. C.* **2009**, *113*, 18946-18952.

[27] B. Seger, G. Q. Lu, L. Z. Wang, *J. Mater. Chem*. **2012**, *22*, 10709-10715.

[28] T. T. Tang, K. Li, D. W. Ying, T. H. Sun, Y. L. Wang, J. P. Jia, *Int. J. Hydrogen Energ.* **2014**, *39*, 10258-10266.

[29] Y. Zhou, S. Basu, K. J. Wohlfahrt, S. F. Lee, D. Klenerman, E. D. Laue, A. A. Seshia, *Sensor Actuat B-Chem*. **2016**, *232*, 680-691.

[30] Y. Wang, H. R. Xu, J. P. Luo, J. T. Liu, L. Wang, Y. Fan, S. Yan, Y. Yang, X. X. Cai, *Biosens. Bioelectron*. **2016**, *83*, 319-326.

[31] X. Cheng, R. Chen, X. Zhu, Q. Liao, X. F. He, S. Z. Li, L. Li, *Int. J. Hydrogen Energ*. **2016**, 41, 2457-2465.

[32] R. Chen, X. Cheng, X. Zhu, Q. Liao, L. An, D. D. Ye, X. F. He, Z. B. Wang, *Chem. Eng. J.* **2017**, *316*, 911-918.

[33] M. Xia, R. Chen, X. Zhu, Q. Liao, L. An, Z. B. Wang, X. F. He, L. Jiao, *Sci. Bull.* **2016**, *61*, 1699-1710.

[34] S. Tominaka, S. Ohta, T. Osaka, R. Alkire, *Energ. Environ. Sci*. **2011**, *4*, 162-171.

[35] S. Tominaka, S. Ohta, H. Obata, T. Momma, T. Osaka, *J. Am. Chem. Soc*. **2008**, *130*, 10456-10457.

[36] M. Antoniadou, S. Sfaelou, P. Lianos, *Chem. Eng. J.* **2014**, 254, 245-251.

[37] E.R. Choban, J.S. Spendelow, L. Gancs, A. Wieckowski, P.J.A. Kenis, *Electrochim. Acta*. **2005**, 50, 5390-5398.

[38] Y. Li, J. Lv, Y.L. He, *J. Electrochem. Soc.* **2016**, 163, F424-F427.

[39] L. Li, S Xue, R. Chen, Q. Liao, X. Zhu, Z.B. Wang, X.F. He, H. Feng, X. Cheng, *Electrochim. Acta* **2015**, 182, 280-288.

Figure captions

Fig. 1 Illustration of (a) design and (b) picture of the developed μPFC.

Fig. 2 The SEM results of (a) TiO_2 porous layer and (b) quantum dots photosensitized TiO_2 porous layer.

Fig. 3 UV-Vis absorption spectra of the CdS-ZnS/TiO_2 and TiO_2 porous layers.

Fig. 4 (a) Photo-voltage response and (b) photo-current response.

Fig. 5 Influence of light intensity: (a) polarization curves and (b) power density curve.

Fig. 6 Influence of methanol concentration: (a) polarization curve and (b) power density curve.

Fig. 7 Influence of electrolyte concentration: (a) polarization curve and (b) power density curve.

Fig. 8 Influence of liquid flow rate: (a) polarization curve and (b) power density curve.

Fig. 9 Long-term performance.

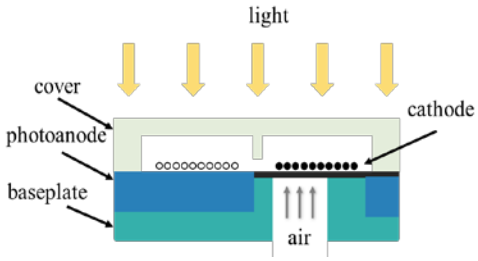

(a)

(b)

Fig. 1 Illustration of (a) design and (b) picture of the developed μPFC.

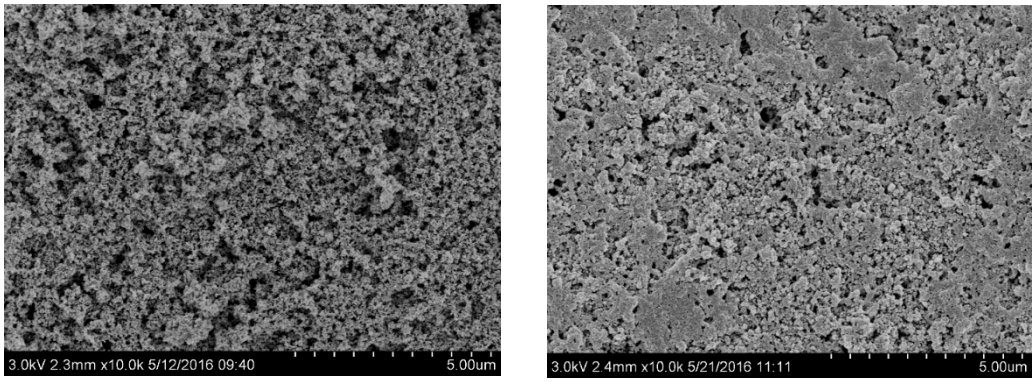

(a) (b)

Fig. 2 The SEM results of (a) TiO_2 porous layer and (b) quantum dots photosensitized TiO_2 porous layer.

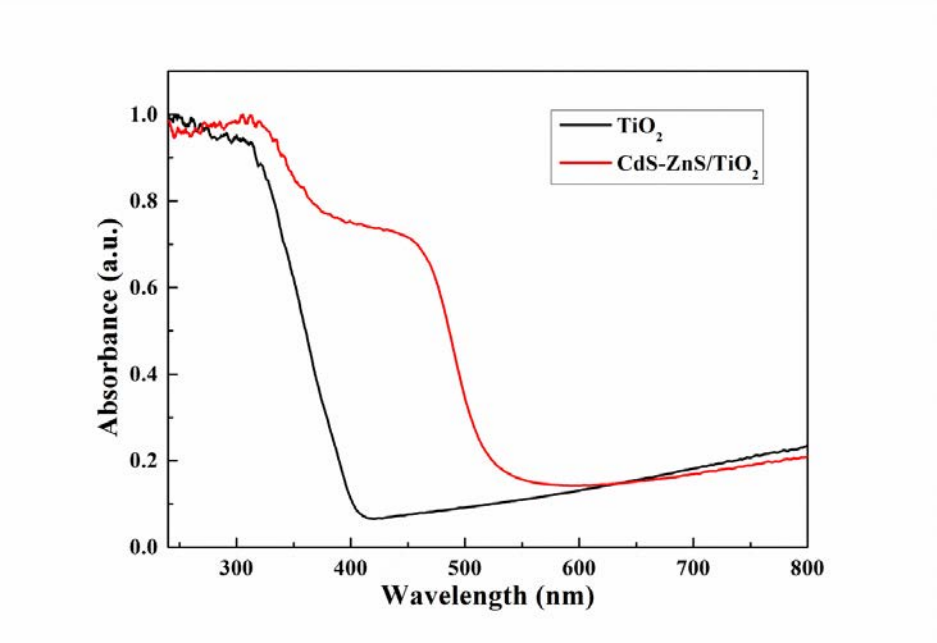

Fig. 3 UV-Vis absorption spectra of the CdS-ZnS/TiO_2 and TiO_2 porous layers.

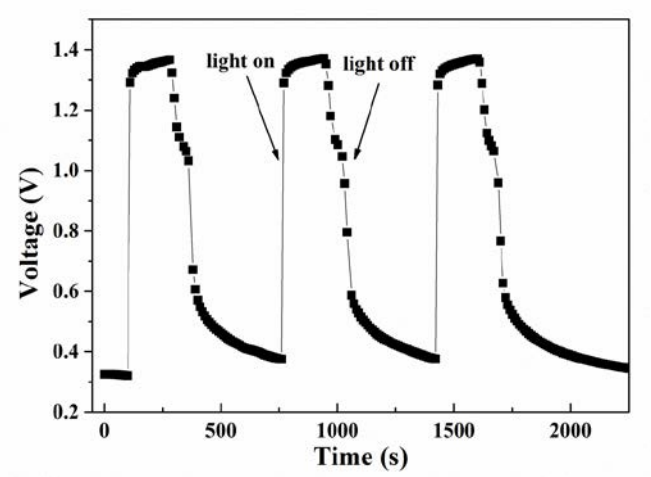

(a)

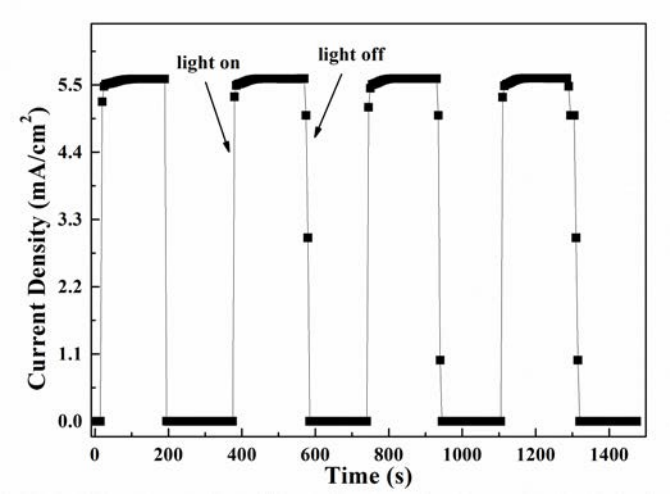

(b)

Fig. 4 (a) Photo-voltage response and (b) photo-current response.

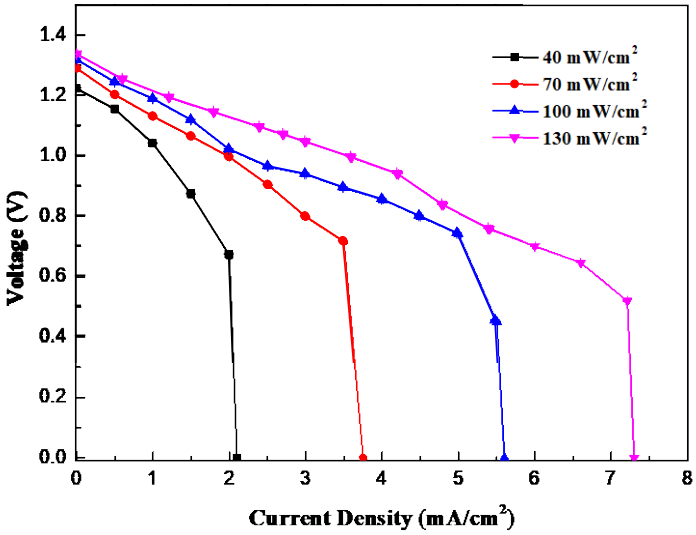

(a)

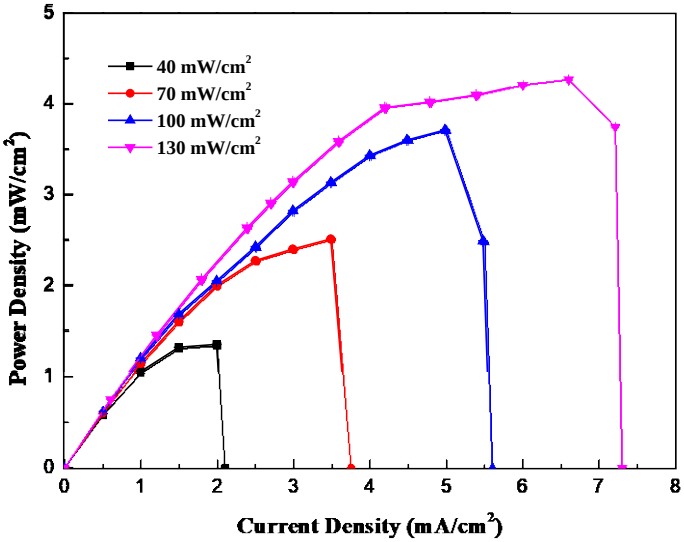

(b)

Fig. 5 Influence of light intensity: (a) polarization curves and (b) power density curve.

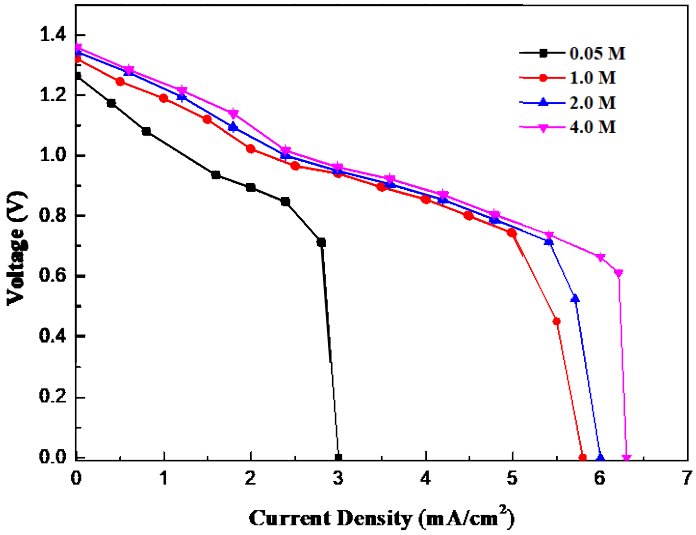

(a)

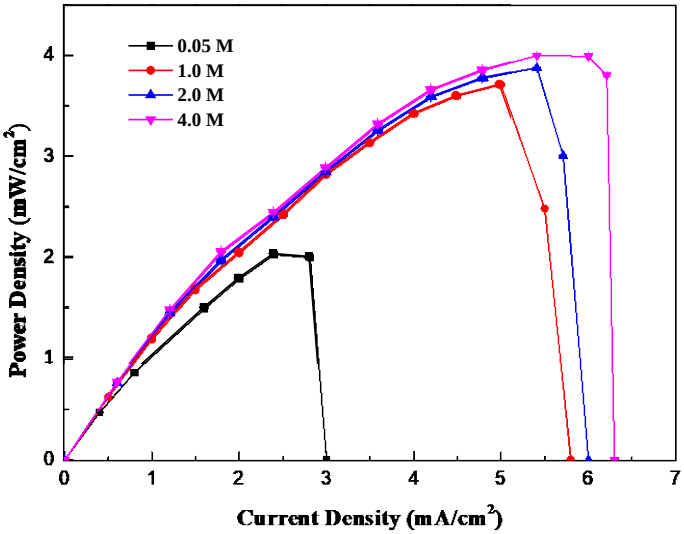

(b)

Fig. 6 Influence of methanol concentration: (a) polarization curve and (b) power density curve.

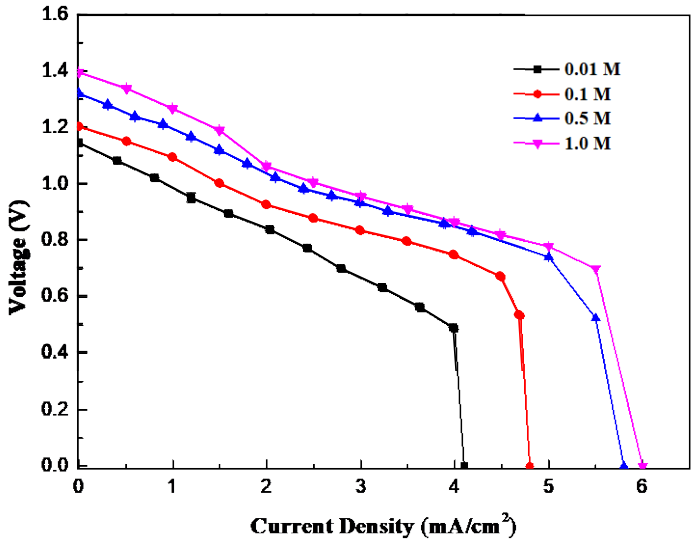

(a)

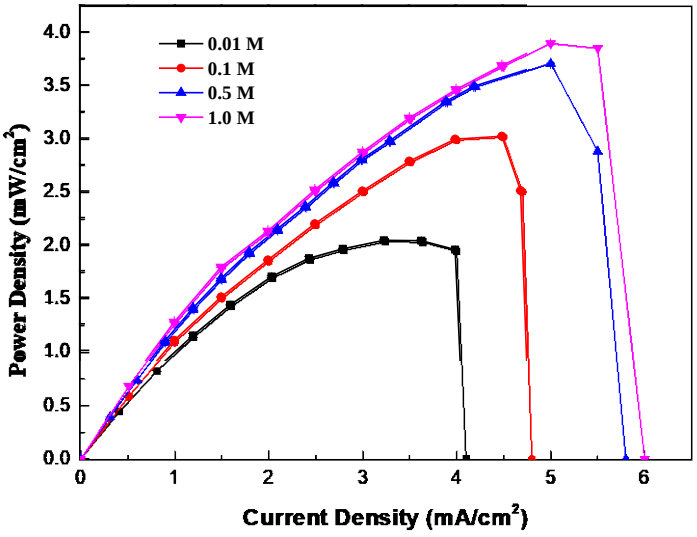

(b)

Fig. 7 Influence of electrolyte concentration: (a) polarization curve and (b) power density curve.

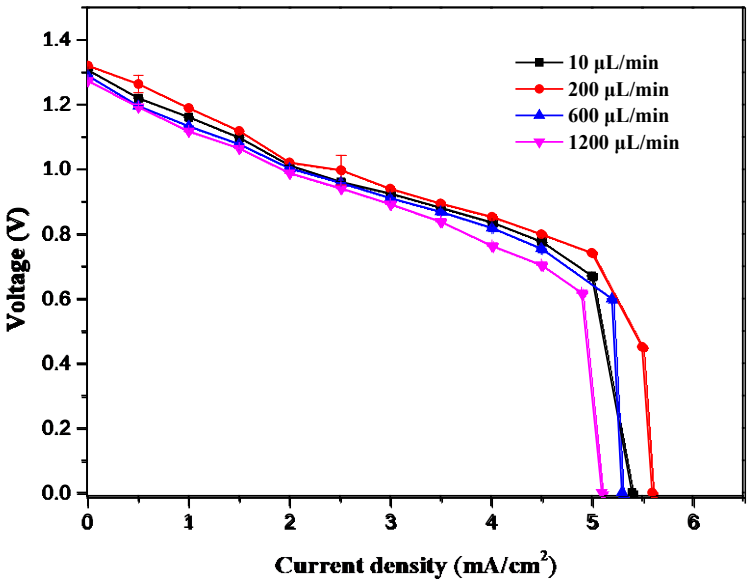

(a)

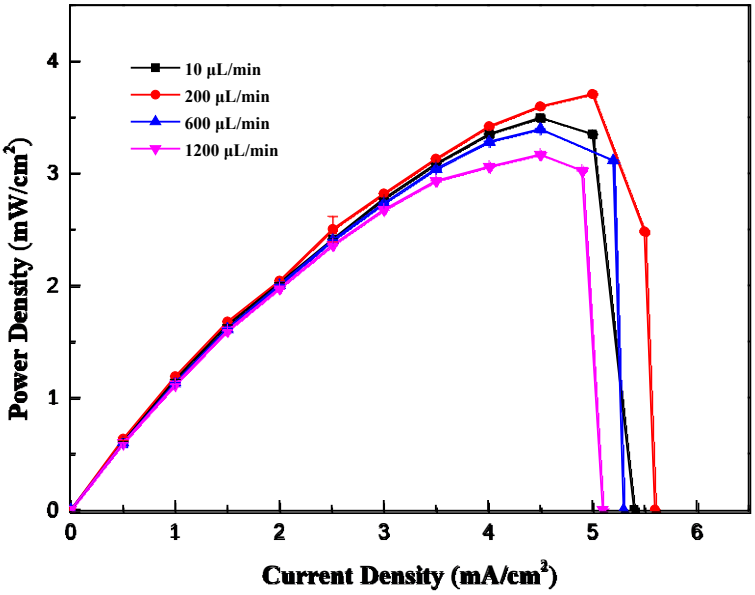

(b)

Fig. 8 Influence of liquid flow rate: (a) polarization curve and (b) power density curve.

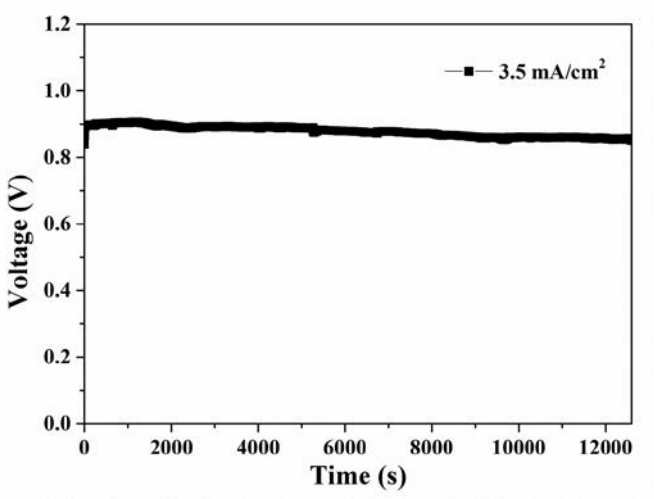

Fig. 9 Long-term performance.